ISSN 1069-3513, Izvestiya, Physics of the Solid Earth, 2006, Vol. 42, No. 7, pp. 551–566. © Pleiades Publishing, Inc., 2006.
Original Russian Text © V.I. Ulomov, T.I. Danilova, N.S. Medvedeva, T.P. Polyakova, 2006, published in Fizika Zemli, 2006, No. 7, pp. 17–33.

Seismogeodynamics of Lineament Structures in the Mountainous Regions Bordering the Scythian-Turan Plate

V. I. Ulomov, T. I. Danilova, N. S. Medvedeva, and T. P. Polyakova

Schmidt Institute of Physics of the Earth, Russian Academy of Sciences,
Bol'shaya Gruzinskaya ul. 10, Moscow, 123995 Russia
e-mail: ulomov@ifz.ru

Received September 30, 2005

Abstract—The Scythian-Turan platform, together with the Alpine Iran–Caucasus–Anatolia and Hercynian Central Tien Shan orogenic structures adjacent to it, represents a coherent seismogeodynamic system responsible for regional seismicity features in the territory under consideration. Investigations of the spatiotemporal and energy evolution of seismogeodynamic processes along the main lineament structures of the orogen reveal characteristic features directly related to the prediction of seismic hazard in this region, as well as in southern European Russia. These characteristics primarily include kinematic features in the sequences of seismic events of various magnitudes and an ordered migration of seismic activation, enabling the more or less reliable determination of the occurrence time intervals (years) and areas of forthcoming large earthquakes (magnitudes of 7.0 ± 0.2, 7.5 ± 0.2, and 8.0 ± 0.2).

PACS numbers: 91.30.Ga

DOI: 10.1134/S1069351306070032

INTRODUCTION

The goal of this work is to study the spatiotemporal and energy evolution of seismic processes along main seismogenic linear structures of the Iran–Caucasus–Anatolia and Central Asia regions and the transition area from the orogenic belt to the Scythian and Turan platforms, which represent a coherent seismogeodynamic system. The extrapolation of seismogeodynamic processes to adjacent territories and the localization of potential sources of large earthquakes is one of the main purposes of our study.

The problem of earthquake occurrence in platform territories, in spite of numerous examples of such seismic events, remains still unsolved in many aspects. This problem is particularly important for densely populated southern European Russia, represented by the geodynamically relatively stable Scythian plate, where only weak and moderate local earthquakes have been known to date. However, the three Gazli earthquakes with the magnitudes M = 7.0 and 7.3 (1976) and 7.2 (1984) took place relatively recently on the Turan plate, adjacent to the Scythian plate and similar to it in deep structure and geological development. (Here and below, the magnitude M means the Ms value determined from surface seismic waves.)

The Scythian and Turan young platforms, having a common epi-Hercynian geological origin, are often considered as the unified Scythian-Turan plate (STP). Seismic manifestations in the STP region are due to the dynamics of the crust and the entire lithosphere of the Iran–Caucasus–Anatolia and Central Tien Shan seismically active regions adjacent to this platform in the south and east. The latter regions are in turn subjected to an intense geodynamic action exerted by the Arabian and Indian lithospheric plates.

The seismic potential is highest in transition zones from orogenic structures to platforms; these zones concentrate geodynamic stresses. The Krasnovodsk earthquake of 1895 (M = 7.9), the largest in western Central Asia; the Ashkhabad catastrophe of 1948 (M = 7.3); and the Balkhan earthquake of 2000 (M = 7.3), which occurred at the western margin of the Turan plate, can serve as examples of strong events on the Turan plate. The three New Madrid earthquakes of 1811–1812 ($M \approx$ 8.0), which occurred during two months in the Mississippi River valley, have long become the classical examples of large platform earthquakes in other regions. The catastrophic earthquake of October 8, 2005 (M = 7.6), in the western piedmont of the Alpine Himalayas (Pakistan), near the northern boundary of the Indian plate, can be mentioned as one of the recent seismic events.

Our studies are based on the new notions of the seismogeodynamics of seismically active regions and their main structural elements that were developed in previous investigations of seismic zoning and prediction of seismic hazard [Ulomov, 1999; Ulomov and Shumilina, 1999].

SPATIOTEMPORAL AND ENERGY EVOLUTION OF SEISMOGEODYNAMIC PROCESSES

Initial Data and Methods of Study

Numerous publications, including ones by the authors of this paper, are devoted to the geodynamics

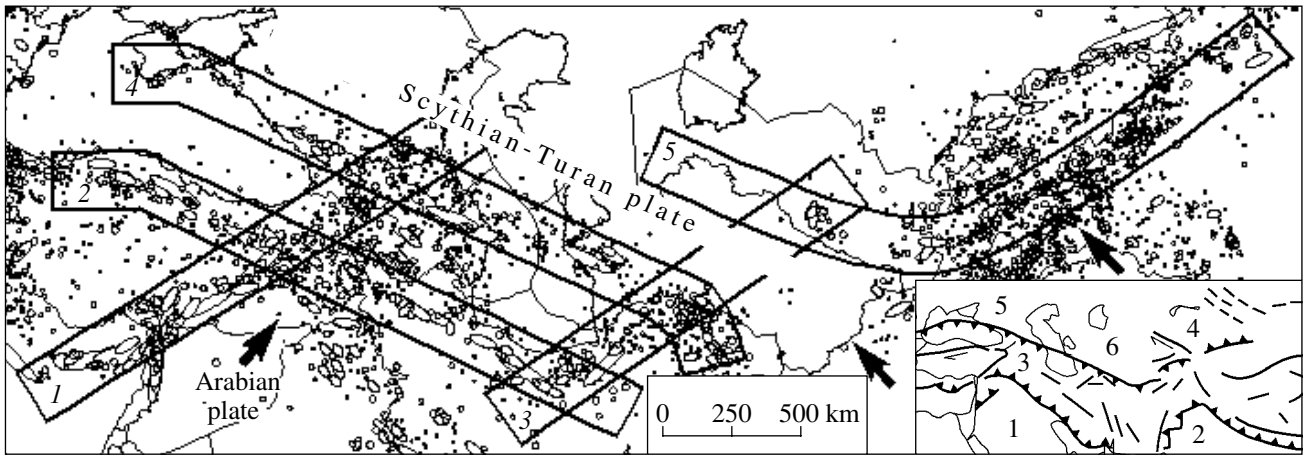

Fig. 1. Position of profiles (bands) along which the spatiotemporal and energy evolution of seismogeodynamic processes was studied: (*1*) Cyprus–Caucasus, 1870 km long; (*2*) Anatolia–Elburz, 2270 km; (*3*) Elburz–Turan, 1520 km; (*4*) Crimea–Kopet Dagh, 2500 km; (*5*) South Tien Shan, 2520 km. The arrows show the direction of compressive forces exerted by the Arabian and Indian plates. The inset in the bottom right-hand corner shows the main geostructures in the territory studied: 1, Arabian plate; 2, Indian plate; 3, Iran–Caucasus–Anatolia region; 4, Central Tien Shan region; 5, Scythian plate; 6, Turan plate.

and seismicity of the Iran–Caucasus–Anatolia region and the Central Tien Shan [Ulomov, 1974, 1983, 1986; Polyakova, 1985; Ulomov et al., 1999, 2002, 2005]. As was shown in these studies, lineaments ("seismic sutures," according to G.A. Gamburtsev) are the main seismogenic structural elements of the regions. These structures form the framework of all models of earthquake sources. Their dimensions control the magnitude of maximum possible earthquakes in a given region. Seismic lineaments are characterized by the highest ordering of earthquake sources in space and rather clearly expressed processes of seismic activation migration along the lineaments, which in turn makes it possible to estimate the seismic potential of the relevant structures and develop methods of long-term prediction of a seismic situation.

The development of seismogeodynamic processes was studied along the profiles shown in Fig. 1 as bands encompassing the most structured seismicity and the related seismic lineaments.

Each band is about 200 km wide and 2000 ± 500 km long. The sources of all known earthquakes with magnitudes of $M = 6.8$ and more are shown as ellipses reflecting the real orientations and lengths of such sources. They are grouped (normalized) in intervals of 0.5 ± 0.2 magnitude units (7.0 ± 0.2, 7.5 ± 0.2, 8.0 ± 0.2, and 8.5 ± 0.2). The epicenters of earthquakes with magnitudes from 6.5 ± 0.2 to 4.5 ± 0.2 are shown by circles. Catalogs of the largest seismic events ($M \geq 6.8$) that occurred over the period 1800–2004 along each of the considered bands are presented in Table 1.

As noted above, the choice of the profiles was based on the most structured seismicity of lineament structures and information on regional fault–block tectonics, interpretation of cosmic photographs, and analysis of geophysical fields (primarily, isostatic gravity anomalies and their gradients). The strikes of nearly all profiles under consideration are reliably substantiated by geological, geophysical, and seismological data. An exception is the Elburz–Turan profile, which we specified in the central Turan platform after the Gazli earthquakes of 1976 [Ulomov, 1983; Polyakova, 1985].

The Elburz–Turan profile was specified in order to gain insights into the position of the large sources of these earthquakes, which obviously belonged to the western continuation of the South Tien Shan profile but occurred seemingly too far from the similar sources of the 1907 Karatag earthquakes, related to the same seismogenic zone. The intersection of these two seismic sutures was supposed to play a certain role in the occurrence of the Gazli earthquakes because it is known that the largest earthquakes occur precisely at such fault nodes. A hypothetical seismic source on the Mangyshlak Peninsula identified from ancient faults and possibly also confined to the intersection of the NW continuation of the South Tien Shan with the NE continuation of the Cyprus–Caucasus profile is still to be explained from this standpoint.

As seen from Fig. 1, the Cyprus–Caucasus (*1*) and Elburz–Turan (*3*) profiles extend along the direction of geodynamic forces produced by the Arabian plate (the left arrow), and the three other profiles, Anatolia–Elburz (*2*), Crimea–Kopet Dagh (*4*), and the western South Tien Shan (*5*), trend across the direction of these forces. The western part of the latter profile trends along the direction of forces developed by the Indian plate (the right-hand arrows). The Scythian and Turan parts of the STP, contacting with the orogens, are subjected to the corresponding geodynamic effects.

The seismic regime within each profile was examined on the basis of samples of seismic events selected from the summarized catalog that belong to the corre-

Table 1

Date	Coordinates		*h*, km	*Ms*	Date	Coordinates		*h*, km	*Ms*
	φ°, N	λ°, E				φ°, N	λ°, E		
Cyprus–Caucasus					Elburz–Turan				
Aug. 13, 1822	36.60	36.70	17	7.4	Mar. 27, 1830	35.70	52.50	18	7.1
Apr. 2, 1872	36.30	36.40	28	7.3	July 11, 1890	36.60	54.70	14	7.2
May 3, 1874	38.50	39.50	14	7.1	May 1, 1929	37.80	57.80	20	7.2
Mar. 31, 1893	38.30	38.50	21	7.0	Oct. 5, 1948	37.95	58.32	18	7.3
Dec. 4, 1905	38.12	38.63	16	6.8	July 2, 1957	36.10	52.70	21	7.0
Sept. 13, 1924	40.00	41.90	10	6.9	Apr. 8, 1976	40.33	63.67	30	7.0
Dec. 26, 1939	39.80	39.40	13	7.8	May 17, 1976	40.28	63.38	30	7.3
Aug. 19, 1966	39.17	41.56	24	6.8	May 19, 1984	40.38	63.36	15	7.2
May 22, 1971	38.85	40.52	21	6.8	Crimea–Kopet Dagh				
Oct. 30, 1983	40.31	42.10	15	6.8	1851	36.80	58.40	15	6.9
Dec. 7, 1988	40.90	44.20	5	6.9	Dec. 23, 1871	37.40	58.40	28	7.2
Apr. 29, 1991	42.39	43.67	6	6.9	Nov. 17, 1893	37.10	58.40	16	7.1
Anatolia–Elburz					July 8, 1895	39.60	53.70	55	7.9
Mar. 27, 1830	35.70	52.50	18	7.1	Feb. 13, 1902	40.70	48.60	18	6.9
May 13, 1844	37.40	48.00	15	6.9	Sept. 11, 1927	44.30	34.30	17	6.8
June 20, 1866	38.50	41.00	23	6.8	May 1, 1929	37.80	57.80	20	7.2
Mar. 17, 1871	38.00	43.00	32	6.8	Nov. 4, 1946	39.83	54.62	23	7.0
Apr. 28, 1903	39.30	42.30	20	7.0	Oct. 5, 1948	37.95	58.32	18	7.3
Jan. 24, 1916	40.30	36.80	34	7.1	Apr. 29, 1991	42.39	43.67	6	6.9
May 6, 1930	37.50	44.70	20	7.3	Dec. 6, 2000	39.68	54.71	33	7.3
Dec. 26, 1939	39.80	39.40	13	7.8	South Tien Shan				
Dec. 20, 1942	40.70	36.70	11	7.0	Aug. 22, 1902	39.80	76.20	40	7.8
Nov. 26, 1943	41.10	33.70	18	7.3	Oct. 21, 1907	38.50	67.90	35	7.4
Feb. 1, 1944	41.40	32.70	15	7.3	Oct. 21, 1907	38.70	68.10	24	7.3
Aug. 13, 1951	40.90	32.90	17	6.8	Feb. 23, 1949	41.00	83.50	30	7.3
May 26, 1957	40.70	31.00	10	7.1	July 10, 1949	39.20	70.80	16	7.4
Sept. 1, 1962	35.60	49.90	29	7.2	Apr. 15, 1955	39.90	74.60	52	7.1
Aug. 19, 1966	39.17	41.56	24	6.8	Aug. 11, 1974	39.39	73.86	18	7.3
July 22, 1967	40.67	30.69	9	7.1	Apr. 8, 1976	40.33	63.67	30	7.0
May 22, 1971	38.85	40.52	21	6.8	May 17, 1976	40.28	63.38	30	7.3
Nov. 24, 1976	39.10	44.00	33	7.5	Nov. 1, 1978	39.39	72.64	20	6.8
June 20, 1990	36.99	49.35	19	7.4	Mar. 19, 1984	40.38	63.36	15	7.2
Aug. 17, 1999	40.85	30.01	10	7.5	Aug. 23, 1985	39.37	75.44	20	7.0
Nov. 12, 1999	41.15	31.19	10	7.2					

sponding profile and are estimated according to their representativeness (completeness and reliability). To study the migration of earthquake sources, earthquake epicenters were projected on the longitudinal axes of the profiles and their distances were measured from the western ends of the latter. Long-term prediction of large earthquakes was made by analyzing the time accumulation of the corresponding seismic events normalized to the magnitude intervals.

Below, we present the information about large earthquakes on each of the profiles under consideration, beginning from ancient times and including the catalogs given in Table 1.

The Cyprus–Caucasus profile (*1*) coincides in strike with the East Anatolian fault and crosses the Caucasus in the NE direction, extending up to Mount Kazbek. The seismotectonics of this segment of the

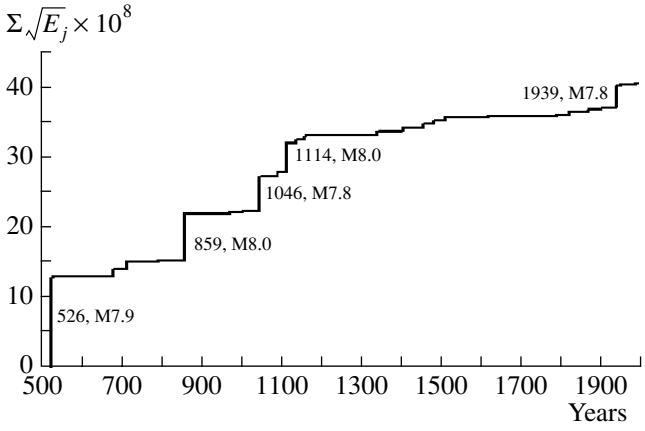

Fig. 2. Benioff cumulative plot for the Cyprus–Caucasus profile. The year of the earthquake and its magnitude are given near the largest events; E_j (joules) is the seismic energy released by earthquake sources.

Alpine fold belt was the object of many investigations [Bune et al., 1976; Polyakova, 1985; Ulomov and Shumilina, 1999] and has been fairly well studied. Earthquake sources are located within the crust all along the profile. Earthquake sources 100–150 km deep are present in the Cyprus area, as well as at the intersection of this profile with the Anatolia–Elburz profile in the area of the town of Erzincan and beneath the Greater Caucasus. The information on strong ($M > 7.0$) earthquakes in the SW part of the profile (in the Cyprus–Levant–Turkey region) has been gathered over a period exceeding three millennia (from 1356 BC). Four earthquakes with $M \geq 7.8$ (526, $M = 7.9$; 859, $M = 8.0$; 1046, $M = 7.8$; and 1114, $M = 8.0$) were revealed here over a historical period of 526–1114. According to historical data, this area is one of the most active areas in the study region. On the other hand, it is noteworthy that no earthquakes, even with magnitudes $M \geq 6.8$, have occurred here since 1900. The last strong earthquakes with $M = 7.3$ and 7.0 occurred in eastern Turkey in 1872 and 1893, respectively. However, the NE part of the profile (to the north from 38°N) became appreciably more active over the period 1900–2004. Numerous earthquakes with $M \geq 6.8$ occurred in Turkey (in 1905, 1924, 1939, 1966, 1971, and 1983) and in Armenia and Georgia (the Spitak earthquake of 1988 and the Racha–Dzhava earthquake of 1991). The Erzincan earthquake of 1939 was the largest ($M = 7.8$). Its source was located at the intersection of the Cyprus–Caucasus and Anatolia–Elburz profiles. The intense release of seismic energy over seven centuries (500–1200), which gave way to a relatively quiescent seismic period of the same duration (1200–1900), is a characteristic feature of the seismicity manifestation along the profile under consideration. This is clearly seen from the Benioff cumulative plot constructed for this profile (Fig. 2).

The Anatolia–Elburz profile (*2*) is characterized by a high seismic potential nearly throughout its length. The seismicity and seismotectonics of North Anatolia have been extensively elucidated in numerous publications. The Iranian part of the profile is also clearly traceable by sources of large earthquakes. Five large earthquakes, of 856 ($M = 8.1$), 958 ($M = 8.0$) (the intersection with the Elburz–Turan profile), 1046 ($M = 7.8$), 1668 ($M = 8.0$), and 1939 ($M = 7.8$) took place within the profile. The 1046 and 1939 earthquakes occurred at the intersection of this profile with the Cyprus–Caucasus profile (*1*). Deep (>50 km) sources of weak earthquakes have been noted in the intersection area. The Anatolian part of the profile is known for strong historical earthquakes of $M = 7.5$–8.0 that occurred in 1419, 1457, 1481, 1509, and 1668. The Erzincan earthquake of 1939 ($M = 7.8$), which was catastrophic for Turkey, and the seismic events of 1942 ($M = 7.0$), 1943 ($M = 7.3$), and 1944 ($M = 7.3$), tracing the North Anatolian fault, are among the earthquakes of the 20th century. Two strong earthquakes of $M = 7.5$ and 7.2 involving vast damage and numerous casualties occurred in 1990 at the western end of the profile in the Izmit area. In northern Iran, this profile is traced by the strongest historical earthquakes of 856 and 958 with magnitudes estimated at $M = 8.0$–8.1, as well as by the earthquakes with $M = 7.5 \pm 0.2$ of 1042, 1550, 1608, 1721, and 1780. In the 20th century, similar earthquakes occurred here in 1976 ($M = 7.5$; Kaldiran, the frontier between Turkey and Iran) and in 1990 ($M = 7.4$; Rudbar, Iran), and their sources filled "gaps" between the sources of historical earthquakes.

The Elburz–Turan profile (*3*) is somewhat tentative, as noted above. This profile was delineated after the Gazli earthquakes of 1976 in the central Turan platform [Bune et al., 1976; Ulomov, 1983; Polyakova, 1985]. This profile is transverse with respect to the strike of the main Alpine geostructures, crosses three longitudinal profiles (*2*, *4, 5*), and breaks into three segments differing in seismic activity. The first, most active, segment extends from the Elburz to the Kopet Dagh inclusive, where it crosses the longitudinal Crimea–Kopet Dagh profile (*4*). The segment next in seismic potential is located at the intersection of this profile with the South Tien Shan profile (*5*), where three Gazli earthquakes ($M = 7.0$, 7.3, and 7.2) occurred in 1976 and 1984 in the same source. They were the largest in the platform. It cannot be ruled out that, if the profile under consideration were extended to the northeast, it would comprise sources of smaller seismic events, including the Chiili earthquake of 1929 with a magnitude of at least $M = 6.5$, whose epicenter was determined insufficiently reliably. Finally, the third segment of the Elburz–Turan profile, between the first two segments, is characterized by a relative geological stability and very weak seismicity, although epicenters of insignificant earthquakes are also met here. The strongest earthquakes within this profile occurred in 856 ($M = 8.1$) and 958 ($M = 8.0$) at its intersection with profile *2*. The large historical earthquakes of ~2000 BC ($M = 7.1$; the Ak-Tepa area), 10 BC ($M = 7.1$; the Nissa area), and

943 (M = 7.6) occurred at the intersection of the Elburz–Turan profile with profile *4*. The Gifan, 1929, and the Ashkhabad, 1948, earthquakes are recent seismic events of identical magnitudes. The latter nearly completely destroyed the capital of Turkmenistan with its population of almost a hundred thousand.

The Crimea–Kopet Dagh profile (*4*) was most comprehensively studied in [Polyakova, 1985; Ulomov et al., 1999, 2002, 2003, 2005; Ulomov, 2003]. Similar to the Anatolia–Elburz profile (*2*), this profile is transverse to the direction of active geodynamic forces developed by the Arabian plate and includes two offshore areas: the NE coastal part of the Black Sea and the central Caspian Sea. This profile, although it is quite distinctly traceable by geological, geophysical, and seismological data, can be divided into four parts. Its western part extends from the Crimea to the middle of the Greater Caucasus and is characterized by relatively rare weak and moderate earthquakes with paleoseismological evidence of very large ancient seismic events. The next part is the seismically active eastern half of the Greater Caucasus, including the area of intersection of this profile with the Cyprus–Caucasus profile. The third, offshore, area comprises the central Caspian Sea. The fourth part includes the Kopet Dagh and the intersection area of the profile under consideration with the Elburz–Turan profile (*3*). Sources of local earthquakes are predominantly located in the crust, and only several sources occur at depths of 50 and even 100 km in the water area of the Caspian Sea, in the Kopet Dagh, and in the eastern Greater Caucasus. The largest earthquakes along this profile occurred on both sides of the Caspian Sea: in 1668 (M = 7.8) in the Shemakha area, in southeastern offshoots of the Greater Caucasus, and in 1895 (M = 7.9) in western Turkmenistan south of the town of Krasnovodsk. In the 20th and the early 21st centuries, earthquakes with M = 7.0–7.5 (±0.2) occurred in the coastal Crimea zone (1927; M = 6.8), the Caucasus (Shemakha, 1902, M = 6.9; Racha, 1991, M = 6.9), and Turkmenistan (Kazandzhik, 1946, M = 7.0; Balkhan, 2000, M = 7.3; the sources of these earthquakes were located to the northeast of the 1895 Krasnovodsk earthquake). At present, seismically active is the zone of the Caspian water area connecting the Cheleken and Apsheron peninsulas. Earthquakes with M = 6.0–6.5 (±0.2) occurred here in 1911, 1931, 1935, 1986, and 1989. The earthquakes of 943 (M = 7.6), 1209 (M = 7.4), 1389 (M = 7.3), and 1405 (M = 7.6) are known to have occurred over the historical period on the Kopet Dagh segment of the profile. The Gifan (Germab), 1929 (M = 7.2), and the Ashkhabad, 1948 (M = 7.3), earthquakes occurred in the 20th century. There is evidence for seismic events of 1100 and 1750 with $M = 7.0 \pm 0.2$ that occurred in the northwestern Greater Caucasus. The Teberda earthquake of 1905 (M = 6.4), the Chkhaltinsk earthquake of 1963 (M = 6.4), and the Racha earthquake of 1991 (M = 6.9) occurred here during the 20th century in places where no earthquakes of such magnitudes had been observed previously. Along with the Yalta earthquake of 1927 (M = 6.8), smaller seismic events including the Anapa earthquake of 800 BC (M = 6.5), the Kerch earthquakes of 63 BC (Ponticapea) (M = 6.4) and 275 (M = 6.4), and the Nizhnyaya Kuban earthquake of 1879 (M = 6.0) are known to have occurred at the NW end of the profile.

The South Tien Shan profile (*5*), in its distinctive configuration and high seismic activity of intracrustal earthquakes, plays the leading role in the Central Tien Shan region [Ulomov, 1974]. This profile extends for 2500 km from the westernmost parts of China to the western frontier of Uzbekistan and, possibly, considerably farther. Comprehensive studies of seismicity of the South Tien Shan, as well as the entire territory of Central Asia, started only at the end of the 19th century. The largest earthquake known within the South Tien Shan region occurred in 1902 in Kashgaria at the Tajikistan–China frontier and had the magnitude M = 7.8. The earthquakes of 1955 (M = 7.1) and 1985 (M = 7.0) occurred in the same place. Two Karatag earthquakes with M = 7.4 and 7.3 occurred one after another in 1907 at the opposite end of the active part of this profile in offshoots of the Hissar Range. Prior to the occurrence of the 1976 and 1984 Gazli earthquakes on the NW continuation of the South Tien Shan, these two events were believed to mark the boundary between the seismically active orogen and the virtually aseismic Turan plate. The Khait (Tajikistan) earthquake of 1949 (M = 7.4), which occurred to the east of the Karatag earthquakes, and the earthquake of 1949 (M = 7.3) in western China, which occurred at the eastern end of the profile under consideration, were large earthquakes. In 1974, the Markansu earthquake (M = 7.3) occurred at the frontier between Tajikistan and China. A fairly strong (M = 6.8) Altai earthquake occurred in 1978 southward of the Fergana Valley. This earthquake is remarkable because it was officially predicted two days before its occurrence on the basis of several (in particular, electromagnetic) precursors that were detected by the prognostic service of Uzbekistan. This successful short-term prediction was recorded in the UNESCO annals, along with the well-known prediction of the Haicheng earthquake of 1975 made by Chinese geophysicists. Previously, the Gazli earthquakes on the Turan plate were predicted at a long-term level ten years before their occurrence [Karzhauv and Ulomov, 1966].

Seismic Regime of Tectonic Sutures

Figure 3 presents the recurrence plots of earthquakes ranging in magnitude from $M = 4.0 \pm 0.2$ to $M = 8.0 \pm 0.2$ that occurred within each of the profiles under consideration. The interval values of magnitudes are plotted on the abscissa axis, and the common logarithms of the average annual number N of the corresponding seismic events are plotted on the ordinate axis. The solid circles show the observed recurrence frequency of such earthquakes determined over time intervals of their representative (most reliable) record-

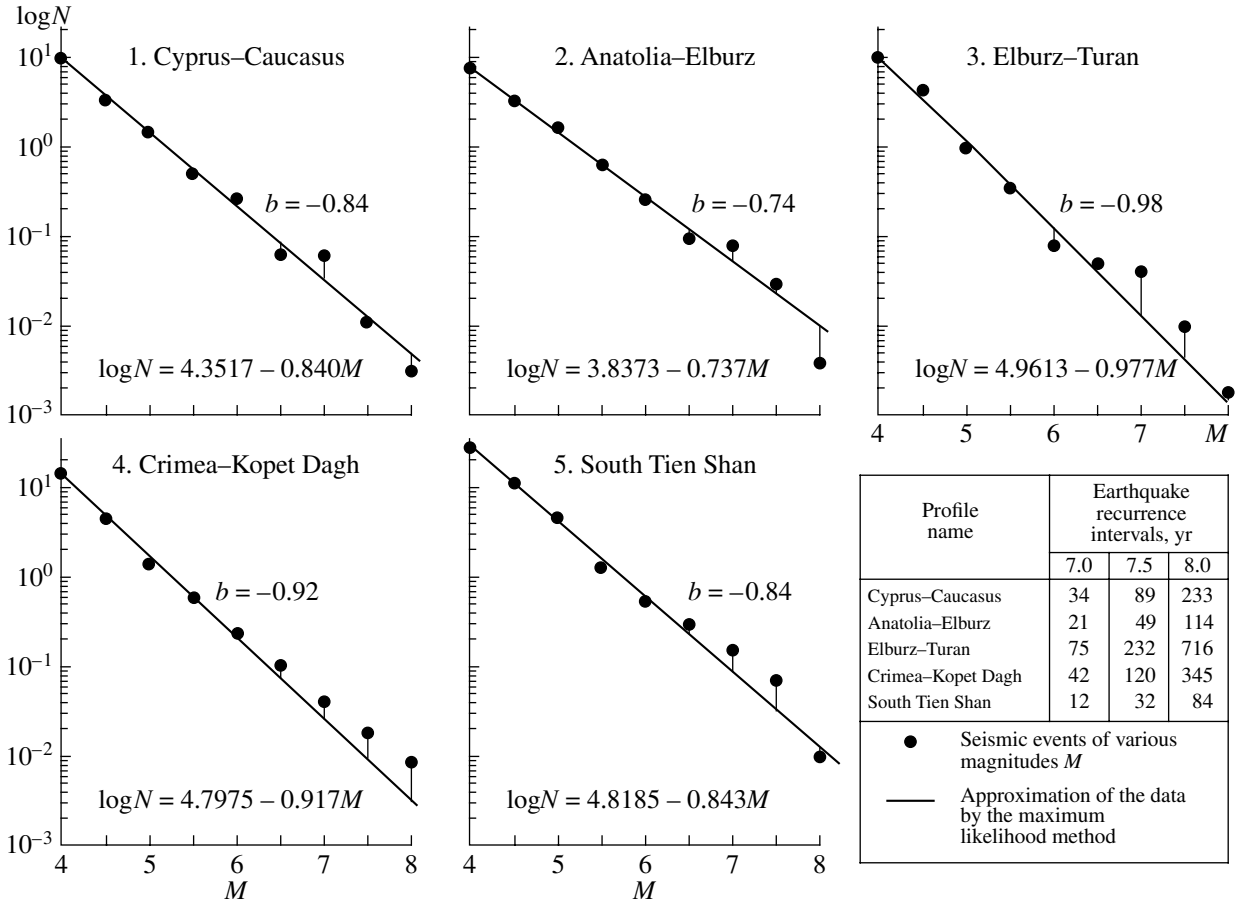

Fig. 3. Interval plots showing the recurrence of earthquakes with $M = (4.0 \pm 0.2)$–(8.0 ± 0.2) within each of the bands under consideration (1–5). The inset in the bottom right-hand corner shows the notation and recurrence intervals of the largest earthquakes with $M = 7.0 \pm 0.2$, 7.5 ± 0.2, and 8.0 ± 0.2.

ing. The straight lines, obtained by the maximum likelihood (ML) method, approximate the points and are described by the equations presented in each plot. In ML applications, larger weights are assigned to numerous and statistically significant weak events, which allows one to reveal deviations of the number of earthquakes with large magnitudes from the approximating log-linear curve (the exponent, on the linear scale). The plots virtually do not change their positions even if the interval of magnitudes is restricted within the limits from $M = 4.0 \pm 0.2$ to $M = 6.0 \pm 0.2$ (the ML property).

As was shown in [Ulomov and Shumilina, 1999], large earthquakes in nearly all regions of North Eurasia occur much more frequently than is "predicted" by the linear extrapolation of the plots toward larger magnitudes. The largest deviations upward from the exponent are usually observed in the magnitude interval 7.0 ± 0.5. Above $M = 7.5$, the observed values of the recurrence frequency again approach the log-linear curve, increasing the slope of the plot (a "right-hand bend"). This phenomenon is observed in nearly all plots of Fig. 3. The underestimation of the observed recurrence of earthquakes with $M = 7.5 \pm 0.2$ along the Cyprus–Caucasus and Anatolia–Elburz profiles looks anomalous in this respect and can point to a deficit of such earthquakes in these structures at present and to a higher probability of their occurrence in the near future. A deficit of events with $M = 6.0 \pm 0.2$ is observed along the Elburz–Turan profile. The recurrence intervals of earthquakes with $M = 7.0 \pm 0.2$, 7.5 ± 0.2, and 8.0 ± 0.2, calculated by the corresponding equations, are presented for each profile in the table in Fig. 3.

The linear slopes b have quite realistic values, indicating the correctness of the choice of dimensions for the profiles under consideration. The value $b \approx -0.7$ for the Anatolia–Elburz profile looks somewhat underestimated, which can be interpreted as less reliable representativeness of weak seismic events compared to earthquakes of larger magnitudes.

Migration of Seismic Activation

A work by the Tashkent geologists and seismologists N.P. Vasil'kovskii, G.V. Popov, and M.P. Repnikov [Vasil'kovskii and Repnikov, 1940] was one of the first scientific publications devoted to migration of

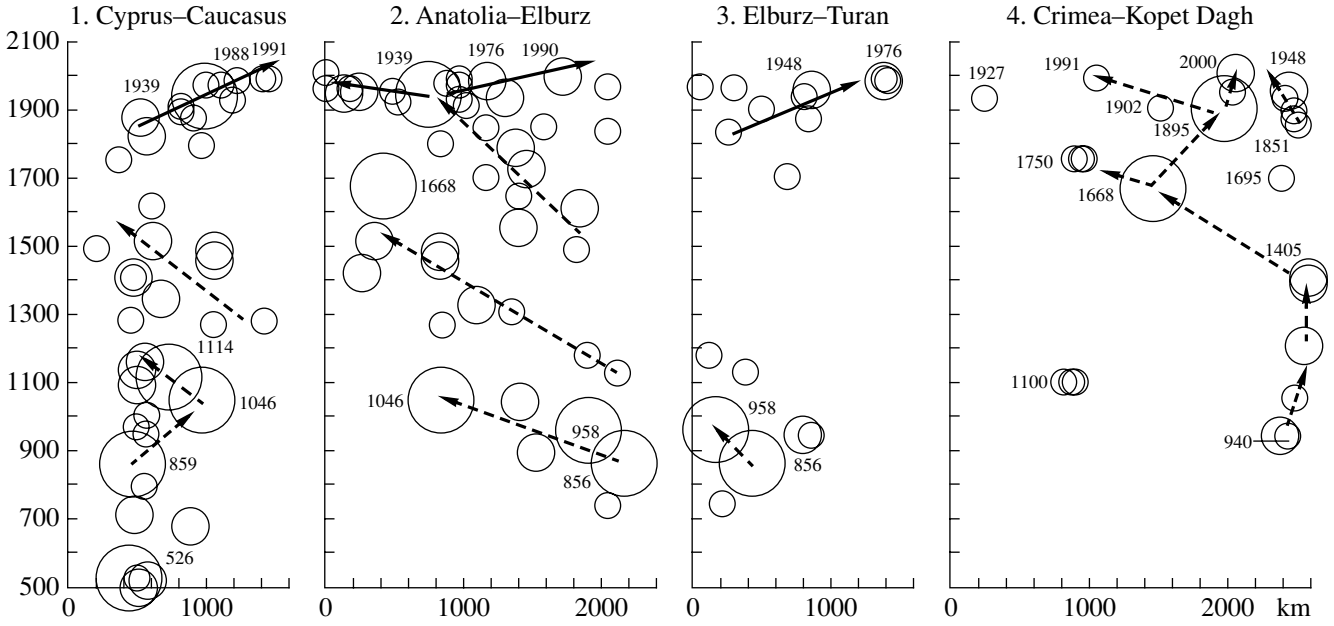

Fig. 4. Spatiotemporal distributions of earthquake sources and the phenomena of seismic activation migration along the Cyprus–Caucasus, Anatolia–Elburz, Elburz–Turan, and Crimea–Kopet Dagh profiles. Years are plotted on the ordinate axis, and the distances along the profiles measured from their western ends are plotted on the abscissa axis. The arrows show the migration directions. The most reliable trends are shown by solid lines and are considered in detail in this work.

earthquake sources. Even at that time, earthquake sequences were considered as interrelated events treated with the use of Markovian chains. Later, these investigations were continued and the migration of seismic sources was interpreted in terms of the propagation of deformation waves triggering earthquakes along seismic lineaments [Butovskaya et al., 1961; Ulomov, 1974, 1983, 1986, 1987, 1988, 1993; Ulomov et al., 2002]. In the concluding section of this paper, we cite numerous publications on this subject by other authors.

The spatiotemporal distributions of seismic sources with $M = 7.0 \pm 0.2$, 7.5 ± 0.2, and 8.0 ± 0.2 that arose during a very long time interval (beginning from 500) along the Cyprus–Caucasus, Anatolia–Elburz, Elburz–Turan, and Crimea–Kopet Dagh profiles are plotted in Fig. 4. The South Tien Shan profile is considered in the next section, presenting more detailed information on the remaining four profiles over the period from 1800 up to the present (see Fig. 6). In this case, the South Tien Shan profile was excluded because, as noted above, more or less reliable information on the seismicity of this territory has become available only since 1865, i.e., since the time of the annexation of Turkestan by Russia.

In Fig. 4, the distances measured from the western ends of the profiles are plotted on the abscissa axis and the occurrence times (years) of seismic events are plotted on the ordinate axis. The circles of various diameters are the sources of all known earthquakes with magnitudes of 7.0 ± 0.2 (small-size circles), 7.5 ± 0.2 (intermediate), and 8.0 ± 0.2 (large). The occurrence years are indicated near the largest and most significant events. The dashed arrows show the directions of a probable migration, and the solid arrows show more reliable trends, considered in detail below.

The Cyprus–Caucasus profile (*1*) is characterized by the longest fairly dense sequence of earthquakes as compared with the other profiles. During the period under consideration, the majority of seismic events occurred in the vicinity of the sources of the largest earthquakes of 526 and 859. In 1046, the source area was displaced northward and later returned to the south. Afterward, up to 1616, seismic events showed a certain scatter, after which 136-year quiescence took place, followed by a dense sequence of events with the most clearly expressed migration in the NE direction.

The Anatolia–Elburz profile (*2*) is characterized by the largest number of earthquakes. Three periodically recurring clusters of migration of seismic events are traceable here over the period from 742, i.e., from the time of the first earthquake with $M \approx 7.0$, to the largest ($M = 7.8$) Erzincan earthquake of 1939. Each of these clusters is approximately 400 yr long (740–1100, 1100–1500, and 1500–1939), but their migration velocities differ (7, 4, and 3 km/yr, respectively). Each of the sequences, beginning in the southeast, is concluded with the largest ($M \approx 8.0$) earthquake in the northwest. The first and third sequences have the same length and end in the epicentral area of the earthquakes of 1046 and 1939. The largest ($M = 8.0$) earthquake occurred in 1668 at the western end of the longest, second sequence. The Erzincan earthquake, which occurred

270 years later (in agreement with the average recurrence interval of such earthquakes along the profile considered), produced two branches of migration: the northwestern, Anatolian, and the southeastern, directed toward the Elburz.

The Elburz–Turan profile (*3*), as noted above, is somewhat hypothetical. The absence of earthquakes of the study magnitudes over a long time interval (from 1177 to 1695, i.e., more than 500 yr) is a characteristic feature of this profile. While it is not surprising that such historical information is absent for the Turan platform, its absence in Iran seems anomalous. In the subsequent period, the catastrophic (M = 7.3) Ashkhabad earthquake of 1948 and the Gazli earthquakes of 1976 (M = 7.0 and 7.3) and 1984 (M = 7.2) were the largest events along this profile. In this connection, it is noteworthy that the studies of the Turan plate seismicity reported in [Karzhauv and Ulomov, 1966; Ulomov, 1974] not only discovered (in 1965) giant open fractures on the Earth's surface in the central Kyzyl Kum Desert that can be interpreted as paleoseismic ruptures but also, based on the observations of their activation during 1965–1975, succeeded in long-term prediction of the Gazli earthquakes.

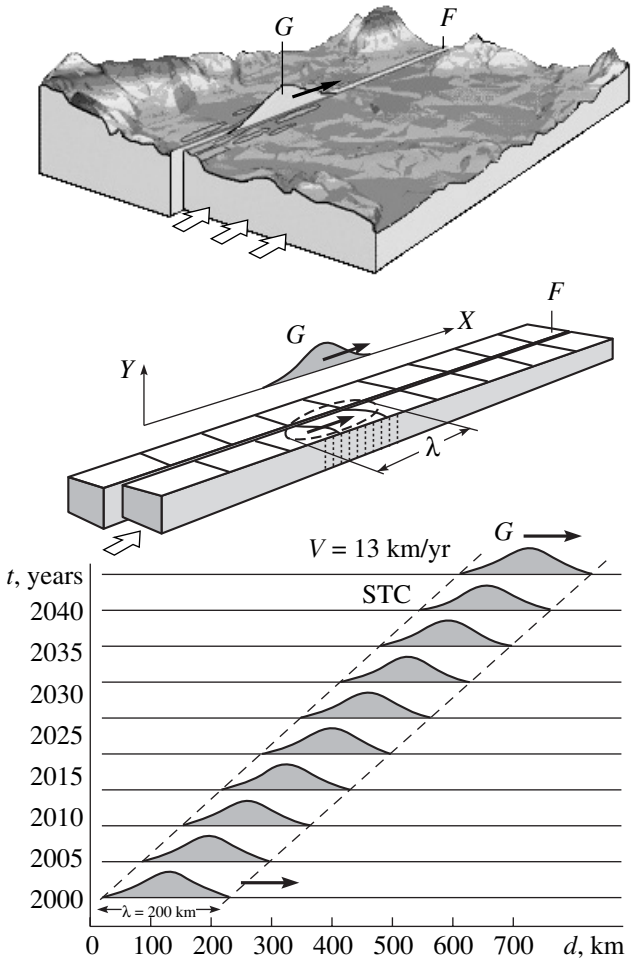

Fig. 5. Movement of the deformation wave G, responsible for migration of the seismic activation region (SAR) along the fault F [Ulomov, 1987]: a 3-D model of the seismic lineament dynamics and a graphic representation of the stress–strain state of the geon G (top); a fragment of the fault zone F, the SAR movement (broken lines), and the $Y(X)$ diagram of the elastic stress gradient (center); and the traveltime curve (space–time channel, STC) of the moving geon G (bottom). The distance along the fault F is denoted by d, V is the velocity of the movement (km/yr), and λ is the wave length of the geon (km). For other explanations, see the text.

The Crimea–Kopet Dagh profile (*4*) is also characterized by diversity of distributions of seismic sources, apparently due to the incomplete seismological information for the Caucasus territory over the past centuries. The information on the Shemakha earthquake of 1668 (M = 7.8) is largely hypothetical, and not all seismologists acknowledge it. The data on a triple earthquake of 1100 with M = 7.0 are also dubious. As regards the cluster of sources that arose in the interval 940–1405 on the eastern termination of the profile, their reliability is much less doubtful because the earthquakes of the cluster occurred on the territory of present-day Iran. However, a nearly 450-year-long (1405–1851) absence of large earthquakes is also observed here. All possible migration paths along this profile are shown by dashed lines, although the strain release in the source of the locally largest Krasnovodsk earthquake of 1895 was quite capable of provoking the Shemakha earthquake of 1902 on the opposite coast of the Caspian Sea and the subsequent migration wave in the NW direction, possibly, up to the source of the Racha–Dzhava earthquake of 1991 (M = 6.9) in Georgia. Evidence for the SE trend toward the Kazandzhik earthquake of 1946 (M = 7.0) and a relatively recent earthquake with M = 7.3 in offshoots of the Great Balkhan Range (western Turkmenistan) is more reliable. It cannot be ruled out that both the 1948 Ashkhabad earthquake and other seismic events in its vicinity closely spaced in time are related to the Krasnovodsk earthquake. The migration processes in this part of the profile under consideration were discussed in detail in [Ulomov et al., 2005b]. The source of the Yalta earthquake of 1927 (M = 6.8) is located somewhat separately on the western termination of the profile.

Geodynamic Model of Migration Processes

Figure 5 illustrates the physical notions concerning the geodynamic nature of the observed migration processes, proposed and discussed in [Ulomov, 1970, 1987, 1993]. The movement direction of the right-hand wall of a fault F under the action of forces applied to it is shown in the upper part of the figure (three large arrows). Since a simultaneous movement of rocks along the entire fault is virtually impossible for energy-related reasons, the stresses and deformations are transferred by parts, i.e., in the form of localized (soliton-like) deformation waves, geons (G) [Ulomov, 1983, 1987]. It is these waves that are responsible for the

dynamics of interacting geoblocks and the direction of the development of seismogeodynamic processes in the fault–block structure of the crust and the entire lithosphere. Propagating along faults, geons successively move their walls. While moving, geons form and break diverse interrock links along the fault, thereby provoking the appearance of earthquake sources.

The dynamics of the fault *F*, clearly elucidating the nature of the continuous-discrete movement of its right-hand wall, is shown in the middle part of Fig. 5. This model further develops the elastic rebound theory of Reid [1911], explaining the mechanism of an individual seismic source, and extends this theory to the entire interconnected set of seismic sources all along an active fault. The analogy between the development of seismogeodynamic processes within individual sources and in large seismogenic zones was noted in [Ulomov, 1974], demonstrating that each individual earthquake with its aftershocks is a model of a large tectonic zone and its behavior in time.

The area shown as the dashed ellipse in the central part of Fig. 5 is similar in the bend of the parallel lines marking the surface of this model to Reid's ideas of the rupture nucleation in an individual source. However, in our case, this is an area of the largest strains and elastic stresses on a local segment of a long fault due to the movement of its right-hand wall. The near segment of the fault, on which earthquakes have already occurred, is shown by two thin lines. The amplitude of displacement is seen from the shifted marks at the "seismic suture" surface. The far segment, still unaffected by displacements, is shown by the thick line. The vertical dashed hatching shows the consolidating sequence in the region of a higher stress–strain state, gradually advancing along the fault. Both slow creep and slips in the earthquake sources arising within this region (called the seismic activation region (SAR) in [Ulomov, 1987]) favor such an advance. In each fragment of Fig. 5, the geon *G* is symbolically shown as the diagram *Y*(*X*) of the gradient of elastic stresses and deformations.

Thus, the geon is a localized region of the consolidating (in the case of compressive geodynamic stresses) or deconsolidating (in the case of extension) volume of the geological medium moving along the fault walls due to slips and creep in the sources of local earthquakes.

The seismogeodynamic potential of the geon ($M^G_{\max}$), controlled by the length, depth, and geodynamics of the corresponding fault–block structure, is determined by the magnitude of the maximum possible earthquake in the latter ($M_{\max}$). The probability of the origination of seismic sources of $M_{\max}$ earthquakes is highest in the central part of the geon. However, such earthquakes can also occur in any other of its parts (frontal, central, or back), depending on the nucleation stage of potential sources.

A moving geon is similar in kinematic parameters to the propagation of ordinary seismic waves, but geons move much more slowly, at velocities ranging from a few to tens and hundreds of km/yr. They are also characterized by a traveltime curve (the lower part of Fig. 5) representing a band called the space–time channel (STC, after [Ulomov, 1987]). Knowing the geon velocity, one can make a long-term prediction of the SAR position corresponding to the geon projection onto the Earth's surface, as well as estimate the magnitude of forthcoming earthquakes and predict their occurrence time intervals (in years).

To illustrate the ordering of the spatiotemporal development of seismogeodynamic processes caused by the movement of geons, the most reliable fragments of the upper parts of the plots shown in Fig. 4 for the Cyprus–Caucasus, Anatolia–Elburz, Elburz–Turan, and South Tien Shan profiles are presented in Fig. 6 on a larger scale. As noted above, a similar analysis for the Crimea–Kopet Dagh profile was performed previously in [Ulomov et al., 2005]. The period from 1820 up to the present time is considered for the first three profiles. The South Tien Shan profile can be studied only since 1865.

The thin broken lines outline the corresponding STCs, and the thick broken lines show the generalized traveltime curves for the corresponding deformation *G* waves characterized by the velocity *V* of seismic activation migration and the wavelength λ. These parameters are specified in each plot in Fig. 6.

As seen from the figure, the migration process of the sources of earthquakes with $M = 7.0 \pm 0.2$, 7.5 ± 0.2, and 8.0 ± 0.2 is most clearly observed along the Cyprus–Caucasus band. The corresponding STC is characterized by a relatively small wavelength ($\lambda = 400$ km) and a low velocity of the geon ($V = 5$ km/yr) as compared with the other profiles considered. The northeastward migration of all sources of earthquakes with the magnitudes under study is clearly observed here over a period of about 250 yr. This migration was best expressed for seismic events with $M = 7.0 \pm 0.2$ after the $M = 7.8$ Erzincan earthquake. The two last earthquakes of this sequence occurred in Armenia (the 1988 Spitak earthquake) and Georgia (the 1991 Racha–Dzhava earthquake) and had the magnitude $M = 6.9$. The earthquake in Georgia was actually predicted in [Ulomov, 1989], where the occurrence area of the forthcoming seismic event of such a magnitude was delineated. It was stated in the same work that the potentially hazardous area extends into the eastern North Caucasus. This hazard exists to date and increases every year.

The seismic migration after the 1939 Erzincan earthquake was no less expressed on the Anatolia–Elburz profile. As regards the western STC branch along the North Anatolian fault, this migration has long become a classical example of this natural phenomenon and has been described in numerous publications. It is

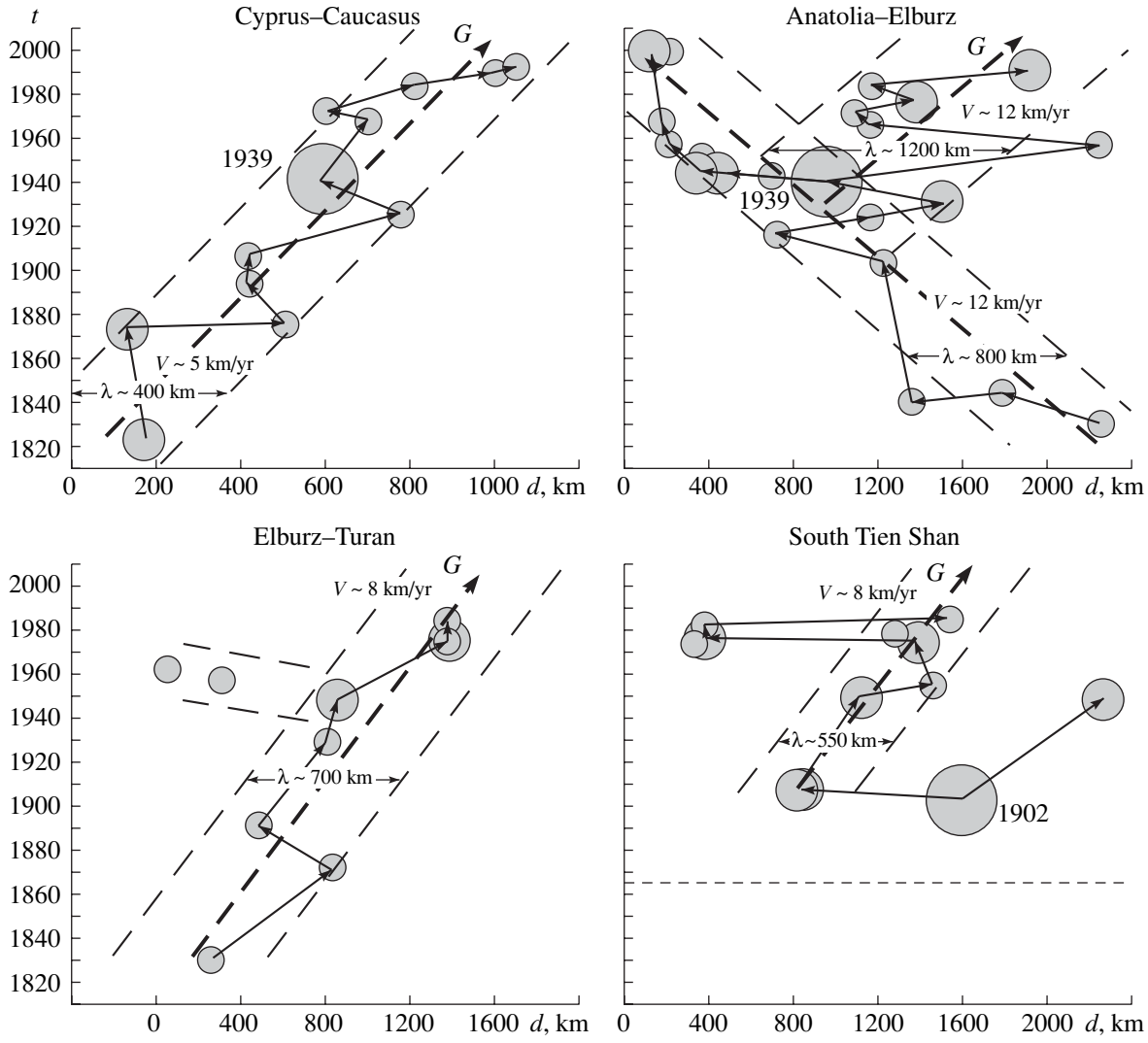

Fig. 6. Migration of seismic activation along the Cyprus–Caucasus, Anatolia–Elburz, Elburz–Turan, and South Tien Shan profiles.

also worth noting that the existence of this STC possibly was longer, which is supported by the sequence of six earthquakes with $M = 7.0 \pm 0.2$ that occurred over 100 years (1830–1930) preceding the Erzincan earthquake. The last earthquake with $M = 7.5 \pm 0.2$ of the eastern branch (events of 1939, 1976, and 1990) occurred in 1990 in Iran.

Origination Succession of Large Earthquake Sources

The cumulative curves approximating sequences of earthquakes of various magnitudes (Fig. 7) clearly reflect specific features of the seismic regime and enable the determination of its average long-term characteristics and the study of spatiotemporal fluctuations caused by the seismogeodynamics along each profile under consideration and in the region as a whole. The comparative analysis of the configurations of such curves and the extrapolation of the sequence of seismic events to the near future open up new opportunities for revealing indicators of nucleation and long-term prediction of large earthquakes [Ulomov et al., 2002, 2005].

Figure 7 illustrates both the accumulation of seismic events in the specified magnitude intervals that occurred in the territory of each profile under consideration and their long-term prediction. The time (t, years) is plotted on the ordinate axis of each plot, and the ordinal numbers (n) of earthquakes in each chronological sequence are plotted on the abscissa axis. The straight lines approximate the entire sets of events of the corresponding magnitudes, and the curves are obtained by the B-spline interpolation of the initial data. Table 2 presents the linear approximation equations (t_M) and correlation coefficients (R^2) of these lines with the initial data, as well as the predicted years of earthquakes (t_p) and more realistic time intervals (years in brackets) of expected earthquakes of the corresponding magnitudes calculated from the equations obtained. It is evi-

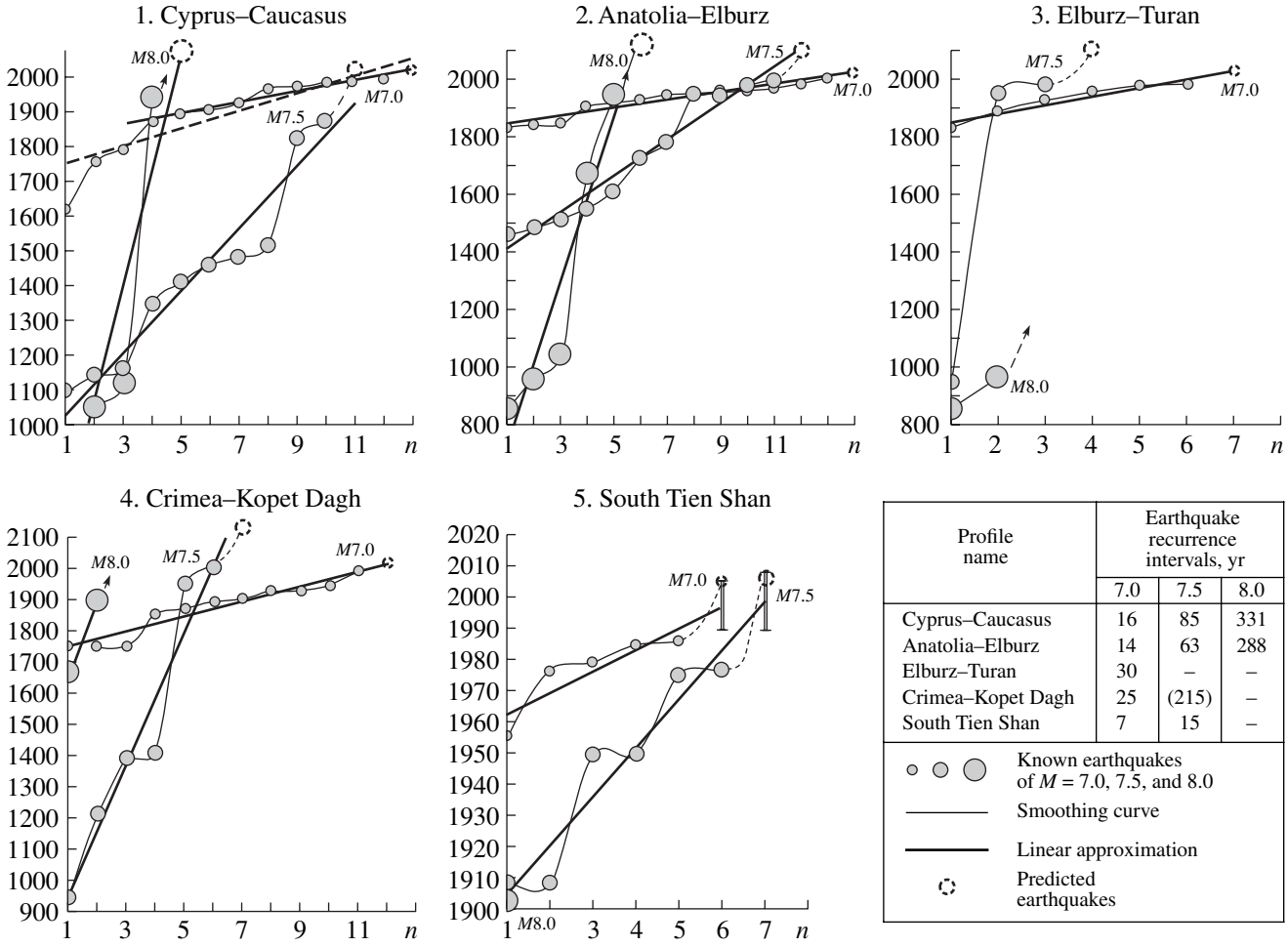

Profile name	Earthquake recurrence intervals, yr		
	7.0	7.5	8.0
Cyprus–Caucasus	16	85	331
Anatolia–Elburz	14	63	288
Elburz–Turan	30	–	–
Crimea–Kopet Dagh	25	(215)	–
South Tien Shan	7	15	–

Known earthquakes of M = 7.0, 7.5, and 8.0
Smoothing curve
Linear approximation
Predicted earthquakes

Fig. 7. Succession of seismic events in the magnitude intervals $M = 7.0 \pm 0.2$, 7.5 ± 0.2, and 8.0 ± 0.2 along the Cyprus–Caucasus, Anatolia–Elburz, Elburz–Turan, Crimea–Kopet Dagh, and South Tien Shan profiles.

dent that all long-term predictions relate to the entire area of a given profile and only if the migration and position of a potential earthquake source are discovered can one speak of a potentially hazardous site in a profile.

The factor at the current number n in each t_M equation, being the slope of each approximating line, determines the recurrence interval of an earthquake of the given magnitude in each sequence of events. The free terms in the equations indicate the year beginning from which the catalog of earthquakes is considered. The solid and open circles show the observed and predicted seismic events, respectively. The occurrence times of the predicted events are calculated by the spline extrapolation. The positions of the open circles in time correspond to the intersections of the splines with the next ("empty") vertical having the number $n + 1$. The recurrence intervals of seismic events of the corresponding magnitudes along each profile are given in the summary table in the same figure.

If seismic events occurred uniformly in time, all of them would be located strictly on straight lines and it would be easy to predict the occurrence times of the next earthquakes. At the same time, although the real picture is not so ideal, it is, nevertheless, characterized by clearly expressed regular features.

Smaller angles of the approximating line (or its segment) are evidence for a higher accumulation rate (i.e., recurrence frequency) of events and, accordingly, a smaller recurrence interval; and vice versa, steeper segments correspond to smaller rates and a rarer occurrence of earthquakes. Therefore, with increasing (decreasing) magnitude, the plots become steeper (flatter).

As seen, nearly all spline curves have a "wavy" configuration, which reflects the general geodynamics of the entire region and its individual parts, incorporating the seismic sutures under consideration. Thus, after an increase in the recurrence frequency of earthquakes, they begin to recur less frequently and a prolonged seismic quiescence is sometimes observed.

The intersection of the ordinate axis by the plots is another noteworthy circumstance. Thus, if the slopes of

Table 2

Number and name of the seismic lineament	Long-term prediction of earthquakes of various magnitudes		
	$M = 7.0$	$M = 7.5$	$M = 8.0$
1. Cyprus–Caucasus	$t_{7.0} = 15.90n + 1816.9$ $R^2 = 0.93$ $t_p = 2024$; 2013–2036 [$t_{7.0} = 25.56n + 1742.1$] [$R^2 = 0.80$] [$t_p = 2049$; 1999–2098]	$t_{7.5} = 90.14n + 1030.2$ $R^2 = 0.95$ $t_p = 1932$; 1860–2003	$t_{8.0} = 331.0n + 412.6$ $R^2 = 0.80$ $t_p = 2068$; 1851–2284
2. Anatolia–Elburz	$t_{7.0} = 13.71n + 1842.4$ $R^2 = 0.92$ $t_p = 2021$; 2005–2036	$t_{7.5} = 62.87n + 1409.5$ $R^2 = 0.95$ $t_p = 2101$; 2056–2146	$t_{8.0} = 287.6n + 718.8$ $R^2 = 0.90$ $t_p = 2157$; 2003–2311
3. Elburz–Turan	$t_{7.0} = 30.15n + 1822.6$ $R^2 = 0.92$ $t_p = 2034$; 2017–2050	–	–
4. Crimea–Kopet Dagh	$t_{7.0} = 24.70n + 1721.3$ $R^2 = 0.92$ $t_p = 2018$; 1994–2041	$t_{7.5} = 214.9n + 730.7$ $R^2 = 0.93$ $t_p = 2235$; 2128–2342	–
5. South Tien Shan	$t_{7.0} = 6.86n + 1955.5$ $R^2 = 0.79$ $t_p = 1997$; 1989–2004	$t_{7.5} = 15.53n + 1889.9$ $R^2 = 0.91$ $t_p = 1999$; 1989–2008	–

the plots objectively reflect the average long-term (short-term, in the case of curves) recurrence intervals of earthquakes of the corresponding magnitudes and are quite suitable for constructing the traditional recurrence plots, the absolute level of the accumulation of events on the time axis is controlled by the representativeness of the initial data used, i.e., by the degree of completeness of earthquake catalogs. This is demonstrated in Fig. 7 by the example of the Cyprus–Caucasus profile, whose plot $M = 7.0$ was constructed in two variants: less reliable, beginning from 1616 (the broken line), and more reliable, beginning from 1874 (the solid line). The anomalous drop of the plot in the interval 1616–1874 illustrates the incompleteness of this part of the catalog. The quantitative characteristics of each variant are given in Table 2. Here, the parameters of the nonrepresentative plot are given in brackets. This plot is seen to have a worse correlation with the initial data and an overly long (nearly 100 years) expectation interval of the next earthquake with $M = 7.0$, whereas the plot that we accepted yields an approximately 20-year prediction interval (from 2013 through 2036) of the most probable occurrence of an $M = 7.0 \pm 0.2$ earthquake along this profile.

Continuing to analyze the process of accumulation of seismic events along the Cyprus–Caucasus profile, we should note that earthquakes with 7.5 ± 0.2 were absent here during 133 years. The last of such earthquakes occurred in 1872 in southern Turkey. The occurrence probability of the next event is rather high. Of course, the seismic quiescence could be longer, as is observed in the period between 1513 and 1824, following frequently recurring earthquakes with $M = 7.5 \pm 0.2$. At present, it is difficult to gain definite constraints for the prediction of the largest seismic events with $M = 8.0 \pm 0.2$ along the profile under consideration. The last of such events, the Erzincan earthquake, occurred in 1939 at the intersection of profiles *1* and *2*. As seen, after two similar earthquakes of 1046 ($M = 7.8$) and 1114 ($M = 8.0$), which occurred in southeastern Turkey, no such earthquakes were observed over more than 800 years before the Erzincan earthquake.

The Anatolia–Elburz profile is highly informative and the most ordered and is characterized by a relatively more reliable predictability of events in all of the magnitude intervals considered. Earthquakes along this profile occur rather uniformly in time, although a sinusoidal behavior is also observable here in the spline approximation of the initial data. The parameters of the pertinent plots are also presented in the table. The occurrence probability of an earthquake with $M = 7.0 \pm 0.2$ in the near future is high. The spline plot possibly starts to rise for events with $M = 7.5 \pm 0.2$, and a more probable occurrence time of such an earthquake lies in the interval 2056–2146. An earthquake with $M = 8.0 \pm 0.2$ is expected not earlier than 2100; however, due to a large scatter in data (2003–2311), it can occur in the near future.

The Elburz–Turan profile (*3*), as noted above, is seismically most inhomogeneous, and it is difficult to predict the development of seismic processes along this profile. The flow of seismic events with $M = 7.0 \pm 0.2$ develops most regularly, and one can state, with a certain degree of confidence, that the occurrence time of

such an earthquake lies in the interval 2017–2050. Nothing definite can be stated as yet concerning the prediction of events with $M = 7.5 \pm 0.2$ and especially with $M = 8.0 \pm 0.2$.

The Crimea–Kopet Dagh profile (*4*) is characterized by a fairly good correlation between the sequences of seismic events with $M = 7.0 \pm 0.2$ and 7.5 ± 0.2. The last events of these sequences occurred relatively recently. These are the Racha–Dzhava earthquake of 1991 ($M = 6.9$) in northern Georgia and the Balkhan earthquake of 2000 ($M = 7.3$) in western Turkmenistan. The former occurred 45 years after the Kazandzhik earthquake of 1946 ($M = 7.0$); the latter, 52 years after the Ashkhabad earthquake of 1948 of the same magnitude, which occurred in the same seismogenic structure. As distinct from rather uniformly recurring earthquakes with $M = 7.0 \pm 0.2$, the four last earthquakes with $M = 7.5 \pm 0.2$ occurred in pairs separated by an interval exceeding 500 yr. The first pair is dated at 1389 ($M = 7.3$) and 1405 ($M = 7.6$); the second pair, at 1948 and 2000. As seen from the table presented in this figure, earthquakes with $M = 7.0 \pm 0.2$ are more likely to occur along this profile in the nearest years. It is difficult as yet to state anything definite concerning events with $M = 8.0 \pm 0.2$.

The grouping of earthquakes with $M = 7.5 \pm 0.2$ is also characteristic of the South Tien Shan profile (*5*), where periodically recurring paired events are clearly observed. These are the double Karatag earthquakes of 1907 with $M = 7.4$ and 7.3; the Chinese ($M = 7.3$) and Khait ($M = 7.4$) earthquakes of 1949; and the Markansu earthquake of 1974 ($M = 7.3$) and the largest Gazli earthquake of 1976 of the same magnitude. Note also that the two last pairs occurred against the background of a decreasing number of events with $M = 7.0 \pm 0.2$ described by the spline curve. As regards prediction, the times of the next earthquakes of the study magnitudes in the South Tien Shan, as seen from the table for this profile, have long expired. Since the Kashgar earthquake of 1902 ($M = 7.8$) is the single known event having the magnitude $M = 8.0 \pm 0.2$, no trend can be identified.

DISCUSSION

Migration of seismic activation has studied by many authors. As mentioned above, the monograph by the Tashkent seismologists and geologists Vasil'kovskii and Repnikov [1940] was a pioneering work. Extensive studies of this subject are reflected in the publications [Butovskaya et al., 1961; Mogi, 1968; Rice, 1969; Ambraseys, 1970; Savage, 1971; Bott and Dean, 1973; Iida, 1974; Anderson, 1975; Kasahara, 1979; Guberman, 1979; Ulomov, 1981; Nikonov, 1984; Malamud and Nikolaevskii, 1989; and others]. We continued and developed such investigations, using linear seismogenic structures of the Iran–Caucasus–Anatolia and Central Asia regions as an example. Some results of our studies are discussed in this paper.

Figure 8, illustrating the source seismicity, shows the position of the profiles studied. As distinct from Fig. 1, only the western part of the South Tien Shan profile, located on the Turan plate, is presented here from technical considerations. Nevertheless, as stated above, the seismogeodynamics of this entire profile is analyzed. In this figure, similar to Fig.1, the sources of all known earthquakes with $M = 7.0 \pm 0.2$, 7.5 ± 0.2, 8.0 ± 0.2, and 8.5 ± 0.2 are shown by ellipses reflecting their real orientations and lengths. The circles of decreasing diameters show epicenters of earthquakes with magnitudes ranging from 6.8 to 4.3. Catalogs of all known seismic events with $M \geq 6.8$ that occurred along each of the considered bands are presented in Table 1.

The sources of earthquakes with $M = 7.0 \pm 0.2$ that occurred beginning from 1900 are blackened. The year and magnitude of the earthquake are given nearby. The two large arrows in Fig. 8 show the direction of geodynamic pressure exerted by the Arabian and Indian (on the right) lithospheric plates, and the smaller arrows show the "forced" movements of crustal zones under the pressure of these plates. The open arrows show the STP "counteraction" to these geodynamic forces. The long dashed arrows show the direction of seismic activation migration revealed above (see Fig. 6).

Our studies showed that mountainous structures of the Iran–Caucasus–Anatolia region and the Central Tien Shan, as well as the STP adjacent to them, represent a unified seismogeodynamic system responsible for seismicity manifestations in the territory under consideration. The study of the spatiotemporal and energy evolution of seismogeodynamic processes along the most clearly expressed linear structures in this territory reveals certain regular features directly related to prediction of seismic hazard, including southern European Russia. These are primarily kinematic features in sequences of seismic events of various magnitudes and dynamically ordered migration of seismic activation. They allow one to determine, with various degrees of reliability, the time intervals (years) and occurrence areas of forthcoming large earthquakes with $M = 7.0 \pm 0.2$, 7.5 ± 0.2, and 8.0 ± 0.2.

The regional regular patterns of the neotectonic development and STP topography forms can be considered as a result of mechanical effects of the adjacent geodynamically active regions. Thus, the Turan experiences lateral pressure from the Pamirs–Hindu Kush and the Tien Shan, whose origin in turn is due to the collision with the Indian plate. The Scythian part of the STP, which includes the plain territories of the Crimea and the Ciscaucasia region and is bounded in the north by the East European platform, is compressed by folded structures of the Greater Caucasus and Mountainous Crimea, whose recent and present movements are controlled by the pressure of the Alpine fold belt, which in turn experiences the pressure of the Arabian plate. The southern part of the Turan platform, contacting with the Alpine mountainous structures of the Kopet Dagh, is

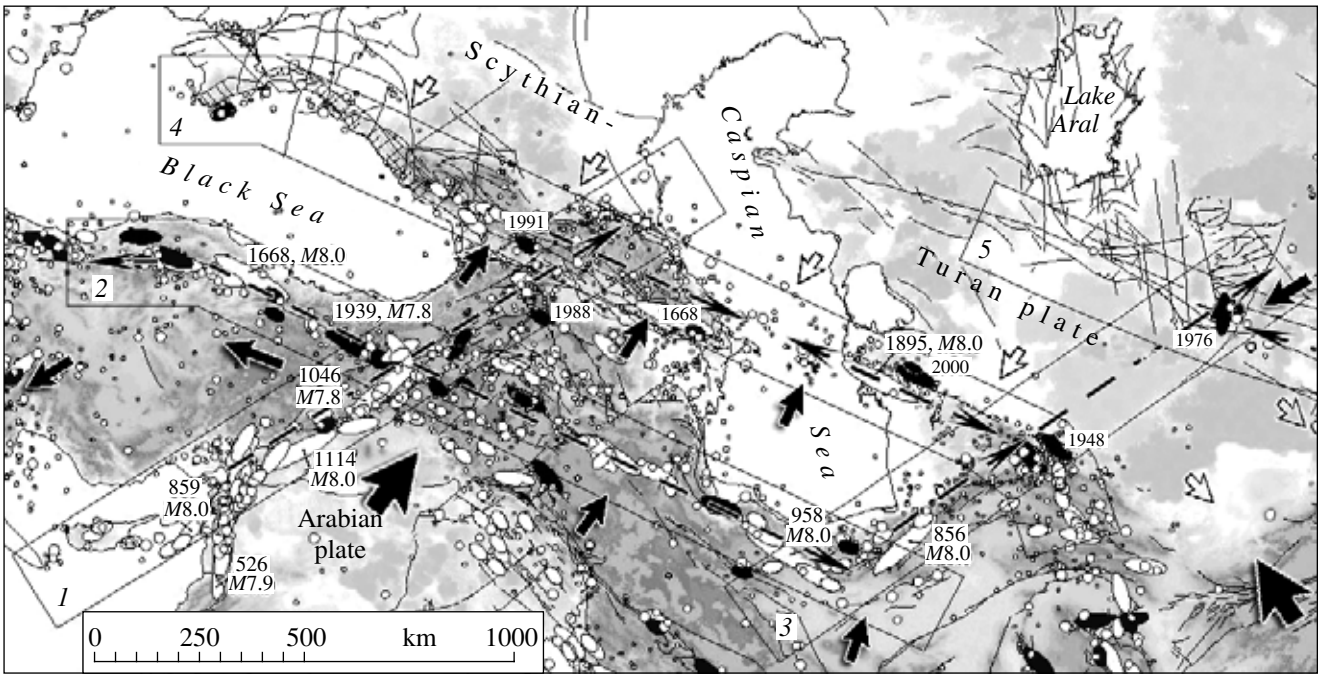

Fig. 8. Seismogeodynamics and seismicity of the mountainous regions adjacent to the Scythian-Turan plate against the topography of the Earth's surface: (*1*)–(*5*) profiles, along which the spatiotemporal and energy evolution of seismogeodynamic processes is studied (see Fig. 1). For other explanations, see the text.

subjected to the same forces of submeridional compression.

We should emphasize that, although the Scythian and Turan parts of the STP, where the cover of platform sedimentary formations overlies rocks of the strongly fractured Hercynian basement, are genetically similar, the orogenic zones of the Iran–Caucasus–Anatolia and Central Asia seismically active regions differ significantly in their strength and geodynamic properties. Thus, the South and Central Tien Shan, formed in the recent time, have an epiplatform origin and are composed of fairly consolidated rocks of the Turan plate, whereas structures of the Crimea, Caucasus, and Kopet Dagh are the youngest Alpine structures, more sensitive to mechanical actions. The latter circumstance indicates that Alpine structures can serve as a kind of a damper absorbing a certain fraction of deformations via the pressure transfer to the Scythian plate and the entire southern part of the ancient East European platform. On the other hand, the pressure exerted by Hindustan on the Central Asia region and, accordingly, the Turan plate is apparently much stronger compared to the pressure of the Arabian plate on Alpine structures of the Crimea–Caucasus–Kopet Dagh region.

These important features can also be responsible for distinctions in seismogeodynamics of individual parts of the territory under consideration, even though the STP and its surrounding mountains represent a unified seismogeodynamic system.

Investigations of the spatiotemporal and energy evolution of seismic processes revealed certain regular features directly related to the analysis of seismogeodynamics and seismic hazard of the territory under consideration. Thus, profiles *1* and *3*, trending across the strike of geological structures and along the forces developed by the Arabian plate, are characterized by a predominantly unidirectional migration of deformation waves, provoking the breakup of links in the sources of nucleating earthquakes and predetermining the direction of seismic migration. In the time interval considered, such a migration had a NE direction. This is most clearly observed along the Cyprus–Caucasus profile. A certain deviation in the position of two seismic sources is detected on the Elburz–Turan profile, in the area of its intersection with the Crimea–Kopet Dagh profile (Figs. 4, 6).

The geological structures along profiles *2* and *4*, orthogonal to the pressure of the Arabian plate, are subjected to horizontal "crushing" responsible for differently directed migration of seismic activity along them. The geodynamic conditions of the South Tien Shan profile (*5*) are no less complex. Here, against a distinct eastward migration of seismic sources observed since the time of the Karatag earthquakes of 1907 [Ulomov, 1974], anomalous westward "pulsations" are present in the form of the Gazli earthquakes and sources in western China (Fig. 6).

As regards long-term prediction of strong earthquakes within the profiles under consideration, the most reliable results are obtained for the Cyprus–Caucasus profile, where a 20-year time interval (2013–2036) of the probable occurrence of an earthquake with

$M = 7.0 \pm 0.2$ has been determined. The NE termination of this profile, i.e., the eastern North Caucasus, is the most hazardous area, in accordance with what is reported in [Ulomov, 1988, 1993; Ulomov and Shumilina, 1999]. The Spitak (1988) and Racha–Dzhava (1991) earthquakes, similar in magnitude to the predicted event, are the predecessors of the event predicted. The 133-year interval of absence of earthquakes with $M = 7.5 \pm 0.2$ is noteworthy on this profile. It is also possible that such an earthquake can occur in this part of the North Caucasus. As yet, nothing definite can be stated concerning the prediction of events with $M = 8.0 \pm 0.2$.

The inferred features of the development of seismic processes, such as the grouping of earthquakes and the sinusoidal shape of the curves approximating the sequences of seismic events in the studied magnitude intervals, are evidence for the existence of deformation waves embracing whole regions.

Further investigations of the ordering in the origination of seismic sources, both in time (recurrence of earthquakes) and in space (distances between sources), will make it possible to identify potential sources more reliably and assess seismic hazard with greater certainty.

ACKNOWLEDGMENTS

We are grateful to G.A. Sobolev for useful comments and I.P. Gabsatarova for providing us with the catalogs of earthquakes recorded by the Geophysical Service of the Russian Academy of Sciences over the past decade in the territory studied. This work was supported by the Russian Foundation for Basic Research, project no. 04-05-64912.

REFERENCES

1. N. N. Ambraseys, "Some Characteristic Features of the Anatolian Fault Zone," Tectonophysics **9**, 143 (1970).
2. D. L. Anderson, "Accelerated Plate Tectonics," Science **187**, 1077–1079 (1975).
3. M. H. P. Bott and D. S. Dean, "Stress Diffusion from Plate Boundaries," Nature **243**, 339–341 (1973).
4. V. I. Bune, V. D. Skaryatin, T. P. Polyakova, and E. I. Shirokova, "Scheme of Tectonic Lineaments and the Distribution of $M \geq 6.3$ Earthquake Sources in the Central Part of the Alpine Fold Belt," Dokl. Akad. Nauk SSSR **230** (6), 1310–1313 (1976).
5. E. M. Butovskaya, A. T. Kon'kov, I. L. Nersesov, et al., *Seismicity of the Fergana Valley* (AN Uz. SSR, Tashkent, 1961) [in Russian].
6. G. A. Gamburtsev, "The State and Prospects of Earthquake Prediction," Byull. Soveta Seismol., No. 1 (1955).
7. Sh. A. Guberman, "D Waves and Earthquakes," in *Theory and Analysis of Seismological Observations (Computational Seismology, Vol. 12)* (Nauka, Moscow, 1979), pp. 158–188 [in Russian].
8. K. Iida, "Slow-Moving Deformation Pulses along Tectonic Faults," Phys. Earth. Planet. Inter., No. 9, 328–337 (1974).
9. T. K. Karzhauv and V. I. Ulomov, "Evidence for Recent Tectonics and Seismicity in the Kyzyl Kum Region," Uzb. Geol. Zh., No. 3, 69–75 (1966).
10. K. Kasahara, "Migration of Crustal Deformation," Tectonophysics **5**, 329–341 (1979).
11. A. S. Malamud and V. N. Nikolaevskii, *Earthquake Cycles and Tectonic Waves* (Donish, Dushanbe, 1989) [in Russian].
12. K. Mogi, "Migration of Seismic Activity," Bull. Earthq. Res. Inst. Tokyo Univ., No. 46, 53–74 (1968).
13. V. N. Nikolaevskii, *Geomechanics and Fluid Dynamics* (Nedra, Moscow, 1996) [in Russian].
14. A. A. Nikonov, *Earthquakes: The Past, The Present, and Prediction* (Znanie, Moscow, 1984) [in Russian].
15. T. P. Polyakova, *Seismicity of the Central Mediterranean Belt* (Nauka, Moscow, 1985) [in Russian].
16. H. F. Reid, "The Elastic Rebound Theory of Earthquakes," Univ. Calif. Publ. Bull. Dept. Geol **6** (1911).
17. J. Rice, "The Mechanics of Earthquake Rupture," in *Physics of the Earth's Interior, Proc. Int. School of Physics "Enrico Fermi," Course 78* (Ital. Phys. Soc., 1969), pp. 555–649.
18. J. C. Savage, "A Theory of Creep Waves Propagating along a Transform Fault," J. Geophys. Res. **76**, 1954–1966 (1971).
19. V. I. Ulomov, "Deformation of Rocks in the Source Area of the Tashkent, April 26, 1966 Earthquake," Izv. Akad. Nauk SSSR, Ser. Fiz. Zemli, No. 9 (1970).
20. V. I. Ulomov, *Dynamics of the Central Asia Crust and Earthquake Prediction* (FAN, Tashkent, 1974) [in Russian].
21. V. I. Ulomov, "Interrelation between the Display of Slow Crustal Movements and Seismicity in Central Asia," Tectonophysics **71**, 191 (1981).
22. V. I. Ulomov, "Plate Tectonics and Seismogeodynamics," in *Experimental Seismology in Uzbekistan* (FAN, Tashkent, 1983), pp. 3–25 [in Russian].
23. V. I. Ulomov, "Seismogeodynamics of the Transition Zone from the Tien Shan Orogenic Belt to the Turan Plate and Long-Term Prediction of the Gazli Earthquakes," in *Gazli Earthquakes of 1976 and 1984* (FAN, Tashkent, 1986), pp. 7–18 [in Russian].
24. V. I. Ulomov, "Synoptic Long-Term Prediction of a Seismic Situation," Dokl. Akad. Nauk UzSSR, No. 6, 47–48 (1987).
25. V. I. Ulomov, "Seismic Hazard Prediction," Arkhit. Stroit. Uzbek., No. 12, 1–3 (1988).
26. V. I. Ulomov, "Seismogeodynamic Activation Waves and Long-Term Prediction of Earthquakes," Fiz. Zemli, No. 4, 43–53 (1993).
27. V. I. Ulomov, "Seismogeodynamics and Seismic Zoning of Northern Eurasia," Vulkanol. Seismol., Nos. 4–5, 6–22 (1999).
28. V. I. Ulomov, "A Three-Dimensional Model of the Lithosphere Dynamics, Seismicity Structure, and Variations in the Caspian Sea Level," Fiz. Zemli, No. 5, 5–17 (2003) [Izvestiya, Phys. Solid Earth **39**, 353–364 (2003)].

29. V. I. Ulomov, "Implication of Horizontal Tectonic Movements for Seismogeodynamics and Seismic Hazard Prediction," Fiz. Zemli, No. 9, 14–30 (2004) [Izvestiya, Phys. Solid Earth **40**, 710–724 (2004).

30. V. I. Ulomov and L. S. Shumilina, *The OSR-97 Set of 1:8 000 000 Maps of the General Seismic Zoning of the Russian Federation Territory. Explanatory Note and the List of Towns and Inhabited Localities Located in Seismically Hazardous Regions* (OIFZ, Moscow, 1999) [in Russian].

31. V. I. Ulomov, T. P. Polyakova, and N. S. Medvedeva, "Seismogeodynamics of the Caspian Sea Region," Fiz. Zemli (1999) [Izvestiya, Phys. Solid Earth **35**, 1036–1042 (1999)].

32. V. I. Ulomov, T. P. Polyakova, and N. S. Medvedeva, "On the Long-Term Prediction of Strong Earthquakes in Central Asia and the Black Sea-Caspian Region," Fiz. Zemli, No. 4, 31–47 (2002) [Izvestiya, Phys. Solid Earth **38**, 276–290 (2002)].

33. V. I. Ulomov, M. Mokhtari, T. P. Polyakova, and N. S. Medvedeva, "Geodynamic Origin of Variations of Seismic Regime of Caspian Area and Level of Caspian Sea," in *Abstracts of 4th Int. Conf. on Seismology and Earthquake Engineering. SEE4. 12–14 May, 2003. Tehran, Paper No. 119* (2003), p. 33.

34. V. I. Ulomov, T. I. Danilova, and N. S. Medvedeva, "On the Development of Seismogeodynamic Processes in the Central Alpine–Himalayan Belt and Central Asia," in *Recent Geodynamics and Hazardous Natural Processes in Central Asia. Proc. All-Russia Conf.* (IZK SO RAN, Irkutsk, 2005), pp. 93–97 [in Russian].

35. V. I. Ulomov, I. P. Kuzin, O. N. Solov'eva, et al., "Seismogeodynamic Migration Processes in the Central Caspian Sea and Adjacent Structures of the Caucasus and Kopet Dagh," Fiz. Zemli, No. 2, 13–22 (2005) [Izvestiya, Phys. Solid Earth **41**, 104–113 (2005)].

36. N. V. Vasil'kovskii and M. P. Repnikov, *Tectonics and Seismicity of the Northeastern Part of the Tashkent Region* (UzFAN, Tashkent, 1940) [in Russian].